International Journal of GEOMATE, July, 2018 Vol.15, Issue 47, pp.1-6
Geotec., Const. Mat. & Env., DOI: https://doi.org/10.21660/2018.47.7308
ISSN: 2186-2982 (Print), 2186-2990 (Online), Japan

LIQUEFACTION SIMULATION FOR THE OSAKA GULF COAST USING THE LIQCA PROGRAM

*Tetsuya Okano[1], Keita Sugito[2] and Ryoichi Fukagawa[3]

[1,2] Graduate School of Science and Engineering, Ritsumeikan University, Japan, [3] Department of Civil Engineering, Ritsumeikan University, Japan

*Corresponding Author, Received: 10June 2017, Revised: 17 Aug. 2017, Accepted: 20 Sept. 2017

ABSTRACT: A Nankai megathrust earthquake is expected to occur in the Kansai area within the next 30–40 years. According to the worst-case estimations by The Headquarters for Earthquake Research Promotion [1], the earthquake will cause economic losses of approximately 220 trillion yen, and 134,000 buildings will be damaged by liquefaction. To estimate future damage to the Osaka gulf coast, we conduct liquefaction simulations based on the LIQCA program developed by the research group at Kyoto University. The liquefiable layers are composed of relatively loose sand and the underground water level is high. The input earthquake motion is the L2 spectrum Ⅰ earthquake-resistant standard spectrum, according to the Design Standards for Railway Structures and Commentary [2]. We consider not only the increase of excess pore water pressure, but also its dissipation. The calculated effective stresses in the sand layers approached 0, after which the sand layers liquefied and unevenness occurred at the ground surface. We evaluated the damage due to liquefaction by calculating vertical displacements and unevenness of the ground surface. Countermeasures are proposed for the shallow sand layers to reduce future liquefaction damage.

Keywords: Liquefaction, Simulation, Nankai megathrust earthquake, Gulf coast, Unevenness

1. INTRODUCTION

A Nankai megathrust earthquake is predicted for the Kansai area within the next 30-40 years. The most recent Nankai megathrust earthquake occurred in 1946 and the recurrence interval of this type of earthquake is over 100 years, according to The Headquarters for Earthquake Research Promotion [1]. If a Nankai megathrust earthquake were to occur, the economic losses would be approximately 220 trillion yen, and 134,000 buildings would be damaged by liquefaction in the worst-case scenario [3], [4]. In addition, a Tokai megathrust earthquake has not occurred for 168 years, even though the recurrence interval of a Tokai megathrust earthquake is also 100 years. It is expected that a Tokai megathrust earthquake would induce the occurrence of a Nankai megathrust earthquake earlier than suggested by its recurrence interval. A Nankai megathrust earthquake would cause huge damage to the Kansai area. Within this area, Osaka city has a significant effect on the national economy and it contains many embankment areas, which tend to liquefy more than other natural ground types. In addition, the high ground water levels of Osaka city would enhance liquefaction.

Therefore, it is important to fully comprehend soil liquefaction characteristics. This paper presents an evaluation of ground liquefaction characteristics for the Osaka Gulf coast. A liquefaction analysis is implemented to assess the liquefaction characteristics. For the scope of this study, the Computer Program for Liquefaction Analysis (LIQCA) is used. This software was developed by the LIQCA Liquefaction Geo-Research Institute (LIQCARI), consisting of researchers from Kyoto and Gifu universities.

2. SIMULATION CONDITIONS

The subject of analysis in this research is a site on the Osaka Gulf coast. A cross sectional view of the study area is shown in Figure 1. The cross section contains an embankment layer, which is approximately 0.4 m to 0.5 m thick. The ground water level is GL-2.3 m.

In this study, we consider the effect of a clay layer (Ac1) and a structure on the liquid sand layer. The influence of the Ac1 layer between the sand layers Bs and As1 is evaluated by considering the thickness of the Ac1 layer. In addition, the influence of a structure is evaluated by comparing the point that bears the load of the structure and the point that does not bear any load. Point A is most affected by the load of the structure and the clay layer Ac1 is thinnest at this point. Point B does not bear the load of the structure and the clay layer Ac1 is thick here. Point C bears some of the load of the structure and the clay layer Ac1 is moderately thick at this point. By comparing the results at these three points, we consider the effect of the clay layer between the liquefaction target layers and the liquefaction damage due to the structure.

Table 1 Material parameters of the R-O model

	Bs	Ac1 Ac2 Ac3	Tc1	Tsg2	Tc2	Oc
	Un-sat.	Sat.	Sat.	Sat.	Sat.	Sat.
ρ	1.8	1.6	1.6	1.8	1.6	1.6
k	1.4 $\times10^{-6}$	9.0 $\times10^{-10}$	2.6 $\times10^{-7}$	1.2 $\times10^{-5}$	1.0 $\times10^{-7}$	7.5 $\times10^{-9}$
e_0	0.658	1.038	0.724	0.777	1.098	1.799
Vs	120	120	200	260	208	208
ν	0.49	0.496	0.494	0.488	0.492	0.492
c (kPa)	0	33	198	0	149	149
φ (deg)	30.9	0	0	34.0	0	0
a	6977	2241	4939	8530	4533	4165
b	0.5	0.5	0.5	0.5	0.5	0.5
α	1.89	-	2.3	2	1.4	1.5
r	1.92	-	2.1	3	1.7	1.6

Table 2 Material parameters of the cyclic elasto-plastic constitutive model

	Bs	As1	As2	Tsg1
	Sat.	Sat.	Sat.	Sat.
ρ	1.8	1.8	1.8	1.8
k	1.5E-6	1.5E-6	1.1E-6	5.2E-6
e_0	0.658	0.990	0.673	0.505
Vs	140	120	170	240
λ	0.002	0.002	0.1	0.001
κ	0.025	0.02	0.02	0.001
OCR*	1.3	1.0	1.0	1.6
G_0/σ'_{m0}	935.5	445.3	646.1	1104
M^*_m	0.909	0.909	0.909	0.909
M^*_f	1.012	0.966	0.958	1.215
B^*_0	3500	2500	5000	10000
B^*_1	80	50	100	200
Cf	0	0	0	0
γ^{P*}	0.02	0.002	0.02	0.005
γ^{E*}_r	0.001	0.3	0.3	0.001
D^*_0	1	1.5	4	4
n	7	2	6	8
C_d	2000	2000	2000	2000

The cross section in Figure 1 includes a structure in the form of a building, modeled as a point load in the LIQCA program. It is hypothesized that this point load will affect liquefaction damage. We evaluate the effect of the load on liquefaction through the presence and absence of the load.

Analysis parameters are based on the Design Standards for Railway Structures and Commentary [2]. LIQCA specific parameters are based on their operating manual. Dynamic parameters are determined using element simulation.

At first, all soil layers are classified as those that determine the target of liquefaction ('Liquefaction-Layers') and those that determine the non-target of liquefaction ('Non-Liquefaction-Layers') based on [2]. Non-Liquefaction Layers are modeled using the Ramberg-Osgood (R-O) model. Liquefaction-Layers are modeled using the cyclic elasto-plasticity constitutive model. The parameters of these models are shown in Table 1 and Table 2, respectively.

The coefficients of permeability k of Bs, As1, As2, and Tsg1 are determined based on a permeability test conducted in the study area. The rest are determined based on the Creager method. The shear wave velocity, Vs, is determined from the Design Standards for Railway Structures and Commentary [2]. The Oc layer is considered as an engineering base surface. The unit weight γ in the Bs, As1, As2, and Tsg1 layers is determined from a mean density soil test in the study area; the rest are determined from the Design Standards for Railway Structures and Commentary [2]. Other specific parameters and the dynamic parameters are determined using the LIQCA program and element simulation.

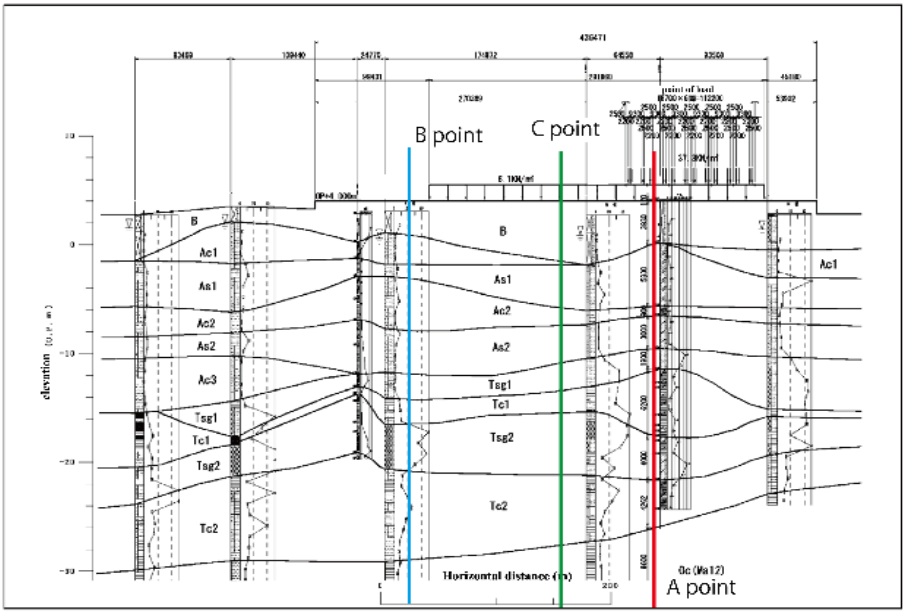

Fig. 1 Cross section of the study area showing the different soil layers.

2.1 Input Seismic Vibration

The input seismic vibration is the H24 L2 earthquake-resistant standard spectrum, shown in Figure 2. It is designed by the Design Standards for Railway Structures and Commentary [2].

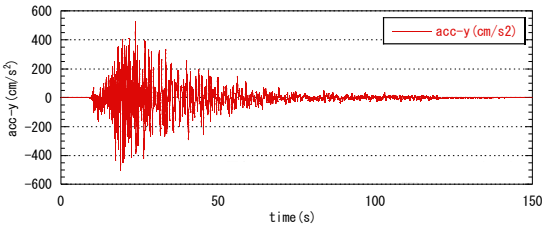

Fig. 2 Input seismic vibration.

2.2 Element Simulation

The specific parameters of Liquefaction-Layers are determined by fitting the liquefaction strength curves from the Design Standards for Railway Structures and Commentary [2]. The specific parameters of Non-Liquefaction-Layers are determined by fitting the dynamic deformation characteristics from the Yasuda-Yamaguchi equations [5].

The liquefaction resistance is regulated by the number of cycles. The liquefaction layer is supported in a simple shear test with a double amplitude of axial strain (DA) of 7.5%, and the number of cycles regulating the strength of the liquefaction is 20. The cyclic shear stress ratios of Bs, As1, As2, and Tsg1 are 0.43, 0.35, 0.31, and 0.31, respectively.

2.3 Initial Conditions

We conduct an initial effective stress analysis, where the mean effective stress with static overburden pressure is analyzed for the case where the coefficient of earth pressure, K_0, is 0.5. All layers are modeled using the Drucker-Prager type plasticity models. Poisson's ratios are determined as 0.33 for K_0 =0.5. The Young's modulus, E, was determined by considering the influence of the effective overburden pressure (Eq. 1), as follows:

$$E = E_0 {\sigma_{m0}}^n \quad (1)$$

$\boldsymbol{E_0}$: Constant of proportionality of Young's modulus (kN/m^2)

$\boldsymbol{\sigma'_{m0}}$: Average effective stress in initial stress state (kN/m^2)

The side boundary condition is the vertical roller support and the bottom boundary condition is fixed. After the effective stress analysis, all displacements and pore water pressures are set to 0.

3. SIMULATION RESULTS

Here, we consider the results in terms of displacements and acceleration, the effective stress reduction ratio, the angle of rotation, and the relationship between effective stress reduction and volume strain, respectively.

3.1 Displacements and Acceleration

Figures 3, 4, and 5 show the time series of the horizontal acceleration response, the horizontal displacement response, and the vertical displacement response, respectively. Table 3 shows the maximum absolute values of displacement and acceleration on the ground surface during shaking. Table 4 shows the displacements on the ground surface during the dissipation stage of excess pore water pressure.

Each horizontal acceleration of the output node is converged. Once again, every output node is selected from the ground surface on the longitudinal plane. After all horizontal accelerations are converged, a dissipation stage of excess pore water pressure analysis is conducted. The time series of horizontal acceleration show the same trend and the maximum absolute value of horizontal acceleration is approximately 2.0 m/s^2 (Figure 3).

Each horizontal displacement of the output node is converged, as with the horizontal accelerations. The maximum absolute value of the horizontal displacement of three output points is approximately 0.847 m. Although the time series of horizontal displacement show the same trend, the final displacements are different (Figure 4). The further to the right the point is on the longitudinal plane, the larger the horizontal displacement.

Again, each vertical displacement of the output node is converged. The vertical sinking was largest at point A, where the clay layer, Ac1, is thinnest (Figure 5). Point B rose slightly due to lateral flow from the thinnest point of the clay layer.

Looking at the time series, when maximum acceleration occurred and the excess pore water pressure rose sharply, the ground surface vibrated slightly. After that, with dissipation of the excess pore water pressure, points A and C experienced vertical sinking. In response to this, the ground surface at point B rose, but subsequently there was slight vertical settlement following dissipation of the excess pore water pressure of the target layer under point B.

Regarding the effect of the structure, the

ground surface of point A and point C dropped significantly under the load. Because of this reaction, the ground surface at point B underwent significant flow. Since the ground surface at point A received a larger load than point C, point A dropped further.

After this, the excess pore water pressure dissipated to between 1×10^4 and 1×10^8 seconds and the ground surface at all points experienced sinking.

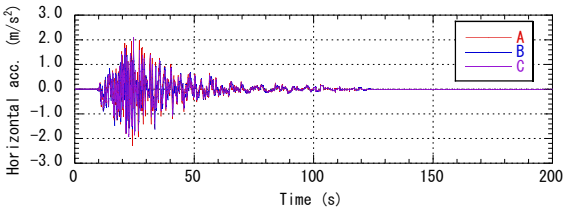

Fig. 3 Time series of the horizontal acceleration response.

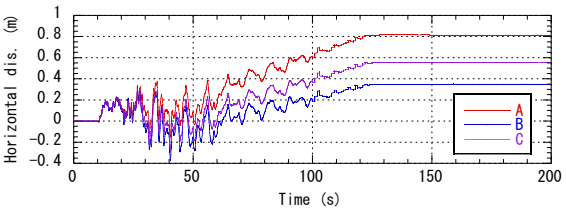

Fig. 4 Time series of the horizontal displacement response.

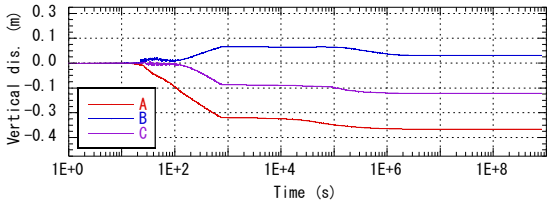

Fig. 5 Time series of the vertical displacement response.

Table 3 Maximum absolute value of displacements and acceleration on the ground surface during shaking

	Displacement (m)		Acceleration (m/s²)
	Horizontal	Vertical	Horizontal
A	0.847	-0.355	2.020
B	0.440	0.088	1.649
C	0.631	-0.163	2.079

Table 4 Displacements on the ground surface during the dissipation stage of excess pore water pressure

	Horizontal displacement (m)	Vertical displacement (m)
A	0.846	-0.355
B	0.437	0.042
C	0.626	-0.162

3.2 Effective Stress Reduction Ratio

Figures 6, 7, 8, and 9 show the effective stress reduction ratio of Bs, As1, As2, and Tsg1, respectively. Table 5 shows the effective stress reduction ratios during shaking. There is no Bs layer at the B output point, so the table does not include the effective stress reduction ratio of the Bs layer.

The excess pore water pressures of the sand, As1, As2, and Tsg1 layers rose more than that of the Bs layer. Because the Bs layer is closer to the ground water level than other sand layers, the excess pore water pressure of the Bs layer dissipated more quickly than that of the other layers.

Regarding the difference between the output points, point B required more time for dissipation of the excess pore water pressure than other points. We consider that the thickness of the upper clay layer is related to the time required for dissipation of the excess pore water pressure. A thicker clay layer results in a longer dissipation time for the sand layer.

Because As1, As2, and Tsg1 layers are above the clay layer, Ac1, their dissipation times are longer than that of the Bs layer.

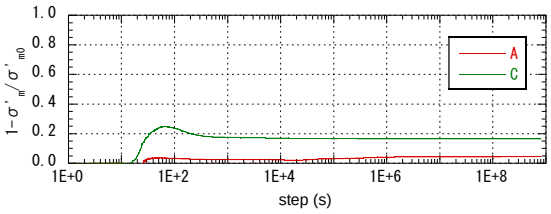

Fig. 6 The effective stress reduction ratio of the Bs layer.

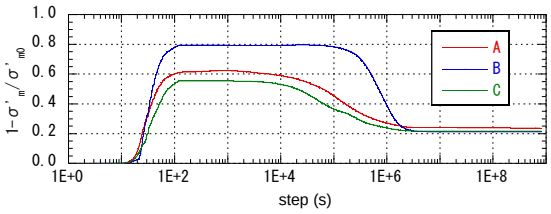

Fig. 7 The effective stress reduction ratio of the As1 layer.

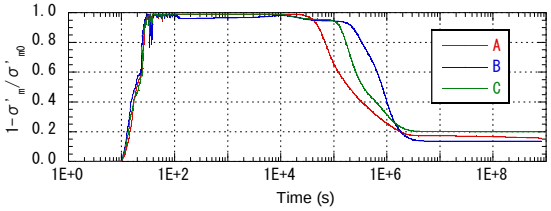

Fig. 8 The effective stress reduction ratio of the As2 layer.

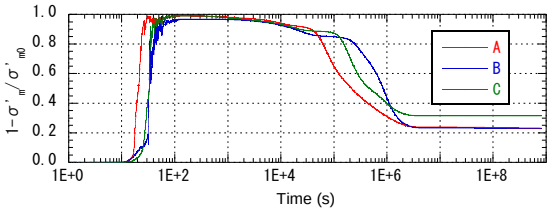

Fig. 9 The effective stress reduction ratio of the Tsg1 layer.

Table 5 Effective stress reduction ratios during shaking

	Bs	As1	As2	Tsg1
A	2.9%	61.3%	98.8%	98.8%
B	-	79.5%	96.1%	96.7%
C	21.1%	55.4%	99.0%	99.0%

3.3 Angle of Rotation

Figures 10 and 11 show the angle of rotation at the ground surface and the vertical displacement at the ground surface, respectively.

The angle of rotation is an index indicating the degree of unevenness. It is an angle represented by the absolute value of a certain node and the angle between two adjacent nodes. For example, it is horizontal when it is 180° and vertical when it is 90°.

The angle of rotation decreased the most around the point at which the load was applied. The ground tilted approximately 0.9° at the point that was most severely affected. Ground unevenness when the shaking ended and when the dissipation stage of excess pore water pressure converged showed the same trend. Therefore, it is considered that liquefaction and loss of strength would occur in a relatively short time.

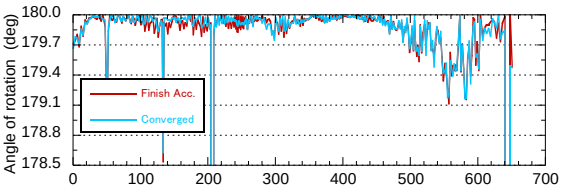

Fig. 10 Angle of rotation at the ground surface.

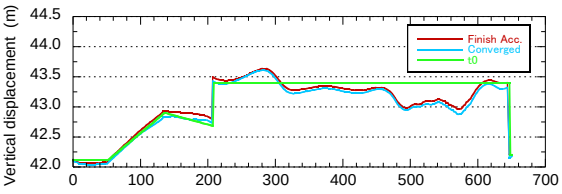

Fig. 11 Vertical displacement at the ground surface.

3.4 Relationship between the Effective Stress Reduction Ratio and Volume Strain

Regarding the excess pore water pressure, the effective stress reduction ratio of the As2 and Tsg1 layers reached 1, indicating liquefaction. This result shows that deeper layers can liquefy. However, the As1 layer and the Bs layer were responsible for significant vertical sinking and horizontal displacement. Figure 12, 13, 14 and 15 show the time series of volume strain of Bs, As1, As2 and Tsg1, respectively. Figure 16 shows the relationship between the effective stress reduction ratio and volume strain. As a result, even though the sand layer at a relatively large depth was liquefied, the amount of volume strain is considered small.

In the study area, the Bs and As1 layers, which are the sand layers near the ground surface, are greatly deformed. Therefore, it is necessary to propose countermeasures.

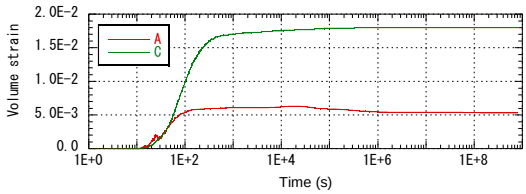

Fig. 12 Time series of volume strain of the Bs layer.

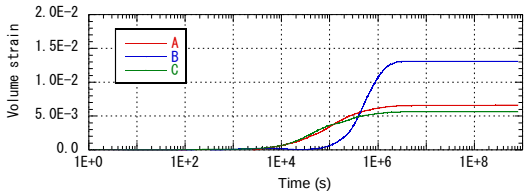

Fig. 13 Time series of volume strain of the As1 layer.

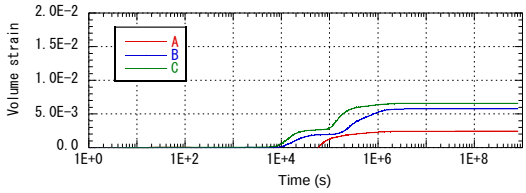

Fig. 14 Time series of volume strain of the As2 layer

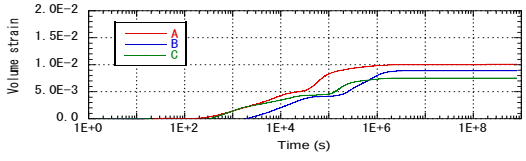

Fig. 15 Time series of volume strain of the Tsg1 layer.

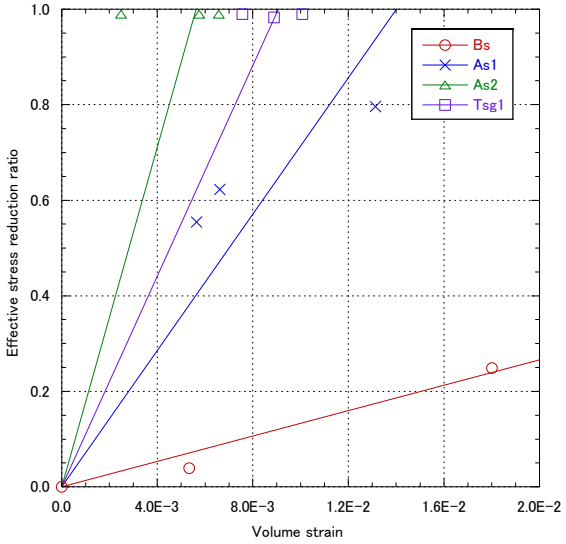

Fig. 16 Relationship between volume strain and the effective stress reduction ratio.

4. CONCLUSION

Liquefaction simulations using the LIQCA program showed that the ground surface on the Osaka gulf coast would sink by a maximum of 0.355 m and move horizontally by a maximum of 0.847 m due to liquefaction. In addition, if there is a structure on the ground surface, the sand would liquefy due to a sudden loss of strength. Conversely, parts of the ground surface would rise as a reaction to the sinking elsewhere.

Shallow sand layers were displaced more than deep sand layers by liquefaction. Regarding the effective stress reduction ratio, the shallow sand layers did not liquefy much, although they did experience significant sinking. The shallow sand layers moved horizontally because Liquefaction-Layers lose strength due to liquefaction. Therefore, the possibility of damage of liquefaction on the ground at Osaka Gulf Coast is considered high.

5. REFERENCES

[1] The Headquarters for Earthquake Research Promotion, “Past earthquake occurrence situation”, Earthquakes occurring in the Nankai Trough, http://www.jishin.go.jp/main/yosokuchizu/kaiko/k_nankai.htm (accessed 2017-06-05)

[2] Railway Technical Research Institute, Design Standards for Railway Structures and Commentary, 2012.

[3] Nihon Keizai Shimbun, Inc., “Estimated damage amount of the Nankai Trough massive earthquake”, Nankai Trough Earthquake, damage amount of up to 220 trillion yen Halved by reduction http://www.nikkei.com/article/DGXNASDG1802L_Y3A310C1000000/ (accessed 2017-06-05)

[4] Disaster Management, Cabinet office, “Aspect of Immediate Disaster”, About the damage estimate of the Nankai Trough massive earthquake, http://www.bousai.go.jp/jishin/nankai/taisaku_wg/pdf/20130318_shiryo2_1.pdf, (accessed 2017-0605)

[5] Yasuda S. and Yamaguchi I., “Dynamic soil properties of undisturbed samples.”, Proceedings of 20th Japan National Conference on Geotechnical, 1985, pp539:542.